Experimental and Theoretical Exploration of the Initial Steps in the Decomposition of a Model Nitramine Energetic Material: Dimethylnitramine

A. Bhattacharya, Y. Q. Guo, and E. R. Bernstein*

Department of Chemistry, Colorado State University, Fort Collins, Colorado

Received: August 13, 2008; Revised Manuscript Received: December 5, 2008

Decomposition of dimethylnitramine (DMNA, $(CH_3)_2NNO_2$) has been studied extensively over the past decades. Although several different mechanisms have been proposed for the initial decomposition of DMNA, the dominant decomposition channel is still far from fully understood. In this report, we collect all the results reported in the literature, along with our new experimental and theoretical results, into a single reference for a sensible comparison in order to reach a general conclusion on DMNA decomposition. In this effort, nanosecond laser, energy resolved spectroscopy and complete active space self-consistent field (CASSCF) calculations are employed. The parent DMNA molecule is electronically excited using two different UV excitation wavelengths, 226 and 193 nm, to initiate the decomposition process. The NO molecule is observed as a major decomposition product with relatively hot (120 K) rotational and cold vibrational distributions by both time-of-flight mass spectrometry and laser induced fluorescence spectroscopy. On the basis of the experimental observations, a nitro−nitrite isomerization mechanism is predicted to be the major channel of decomposition of DMNA in the excited electronic state with a minor contribution from the HONO elimination mechanism. The branching ratio between nitro−nitrite isomerization and HONO elimination channels is estimated to be approximately 1:0.04. CASSCF calculations show that surface crossing (conical intersection) between upper and lower electronic states along the nitro−nitrite isomerization reaction coordinate plays an important role in the overall decomposition of DMNA. Presence of such an $(S_2/S_1)_{CI}$ conical intersection in the nitro−nitrite isomerization reaction coordinate provides a direct nonadiabatic decomposition pathway from the Franck−Condon point of the S_2 surface, which is experimentally accessed by 226 nm photoexcitation. This excited state isomerization takes place through a loose geometry for which the NO_2 moiety interacts with the $(CH_3)_2N$ moiety from a long distance (∼2.8 Å); however, in the ground electronic state, a similar $(S_1/S_0)_{CI}$ conical intersection in this nitro−nitrite isomerization reaction coordinate hinders the isomerization exit channel, rendering NO_2 elimination as the major thermal decomposition channel of DMNA.

I. Introduction

Elucidation of the initial steps in the decomposition of nitramine energetic materials such as RDX (hexahydro-1,3,5-trinitro-1,3,5-triazine) and CL-20 (2,4,6,8,10,12-hexanitro-2,4,6,8,10,12-hexaazaisowurtzitane) from both ground[1] and excited electronic states[2−5] is of special relevance and importance for practical application, fundamental understanding, and improvement and development of these materials. Since even the initial step of the decomposition of these materials is an extremely rapid[6] and exothermic reaction, determination of the mechanisms and dynamics of the dominant decomposition reaction for nitramine energetic materials is still quite challenging.[7] Because of these difficulties, dimethylnitramine (DMNA), $(CH_3)_2NNO_2$, has been studied extensively as a nitramine model system over the past decades. This simple molecule has both structural and electronic properties that are similar to large, more complex nitramine energetic materials and is more amenable to detailed experimental and theoretical studies than are the actual energetic species.

To date, initial decomposition of DMNA has been studied by thermal pyrolysis,[8−10] infrared multiphoton decomposition (IRMPD),[11] UV-photodissociation experiments,[12−15] and quantum mechanical computations.[16] Nonetheless, its decomposition has not proven easy to unravel in determining the dominant reaction pathway, which is still an unresolved problem. As both experimental and theoretical results on DMNA decomposition are widely dispersed in the literature, a review collecting all the results into a single reference seems appropriate and useful.

The main purpose of this report is to present a sensible comparison of widely varied and often confusing experimental and theoretical results on DMNA decomposition. In this effort, to the best of our ability, first, all references that are related to DMNA decomposition will be included in order to provide a complete and comprehensive review. Second, our experimental and theoretical results will be presented and discussed. Third, all the results will be compared and contrasted to reach a general conclusion on the decomposition mechanisms for DMNA.

Our present experimental work focuses on the excited electronic state decomposition of DMNA. We have adopted a photofragmentation/fragment-detection (PF/FD) technique, for which the parent molecule is electronically excited using different UV excitation wavelengths (226 and 193 nm), and subsequently products are detected and their rotational and vibrational distributions are analyzed using either the same laser or a different time delayed laser. Results reported in the literature, for the most part, support NO_2 elimination as the major decomposition channel of DMNA from excited electronic states. In contrast, our experimental observations suggest that the nitro−nitrite isomerization mechanism is favorable for excited

* To whom correspondence should be addressed. E-mail: erb@lamar.colostate.edu.

10.1021/jp807247t CCC: $40.75
Published on Web 01/14/2009

electronic state decomposition of DMNA. We attribute the possible reason of this discrepancy to different experimental conditions, as is discussed in more detail in the General Conclusions section. Another minor decomposition channel for DMNA from excited electronic states is found to be HONO elimination. The approximate branching ratio between nitro−nitrite isomerization and HONO elimination is estimated to be 1:0.04.

Our present theoretical work focuses on both ground and excited electronic state decomposition of DMNA using a complete active space self-consistent field (CASSCF) level of theory. Present computation corroborates the fact that NO_2 elimination is the dominant pathway of thermal (ground electronic state) decomposition of DMNA; however, nitro−nitrite isomerization is the dominant pathway of excited electronic state decomposition of DMNA. Nitro−nitrite isomerization of DMNA takes place through a loose transition state (TS) geometry near a conical intersection between upper and lower electronic states. Presence of such a conical intersection between upper and lower electronic surfaces along the nitro−nitrite isomerization reaction coordinate provides a direct, nonadiabatic dissociation pathway through isomerization, when DMNA evolves from the excited electronic state.

II. Background

Experimental Section. Stewart et al.[8] performed SF_6-sensitized laser pyrolysis of gaseous DMNA at 900 K under collisional conditions. Their observation is consistent with two decomposition pathways: NO_2 elimination and nitro−nitrite isomerization ($(CH_3)_2NNO_2 \rightarrow (CH_3)_2NONO$) followed by dissociation of the extremely weak O−NO bond.

Lazarou and Papagiannakopoulos[11] performed IRMPD of DMNA in a pyrex cell within an effective temperature range of 1060−1250 K and subsequently detected the final products using a mass spectrometer. They concluded that NO_2 elimination is the dominant decomposition channel and no evidence corroborated either the nitro−nitrite isomerization or HONO elimination channel. Their experimental results are in agreement with the molecular beam IRMPD study of Wodke and Lee (unpublished results quoted in ref 2), however, are in apparent disagreement with laser pyrolysis experimental results.[8] They suggest that the apparent disagreement between their IRMPD[11] and laser pyrolysis experimental results[8] is caused by temperature differences that lead to the different vibrational excitations above the $N-NO_2$ bond dissociation energy. Moreover, if the NO_2 elimination channel is in competition with nitro−nitrite isomerization channel in the ground electronic state, the entropy factor can make the NO_2 elimination at high temperature even more favorable than the nitro−nitrite isomerization. By extrapolation of such a consideration, one would then expect a higher branching ratio between a nitro−nitrite isomerization channel and an NO_2 elimination channel at low temperature.

On the contrary, both Lloyd et al.[9] and Fluornoy[10] come to the conclusion that only NO_2 elimination occurs while DMNA is pyrolyzed in a pyrex bulb over the temperature range of 438−525 K. Although both of them conclude that only NO_2 elimination takes place at low temperature, no immediate explanation is given for not observing a nitro−nitrite isomerization channel, which is also expected at low temperature (compare with IRMPD work[11]).

McQuaid et al.[12] dissociated gaseous DMNA at room temperature under almost collisionless condition using nanosecond laser pulses (15 ns fwhm) at 248 nm photoexcitation and observed NO_2 elimination as the major decomposition channel with some evidence of minor channels such as HONO elimination and nitro−nitrite isomerization. The branching ratio between ground state X^2A_1 NO_2 formation and nitro−nitrite isomerization was estimated to be 1.5:0.001.

Stephenson and co-workers[13] dissociated gas-phase DMNA at room temperature under almost collisionless condition using picosecond laser pulses (30 ps fwhm) at 266 nm, and subsequently detected NO_2 by laser-induced fluorescence (LIF) spectroscopy using 532 nm. They observed both ground state and electronically excited NO_2 products with a larger quantum yield of the ground state X^2A_1 NO_2 product. Their time resolved experiment reveals that monophotonic photodissociation of DMNA at 266 nm occurs within 6 ps.

Sausa and co-workers[14] dissociated DMNA in a molecular beam using both 226 and 193 nm laser radiation and subsequently detected an NO product in time-of-flight mass spectrometry (TOFMS). They observed only NO product from decomposition of DMNA at both 226 and 193 nm photoexcitations. Nonetheless, they conclude that NO_2 elimination is the major decomposition channel of DMNA at these two excitation wavelengths because previous experimental results[12] corroborated the same mechanism as the major decomposition channel of DMNA at 248[12] and 266 nm[13] photoexcitations.

On the contrary, in our previous report,[15] we conclude that DMNA decomposition at 226 nm photoexcitation takes place through a nitro−nitrite isomerization mechanism by contrasting the rotational and vibrational distributions of the product NO from photodecomposition of DMNA and that from NO_2 gas at 226 nm.

Therefore, the available experimental results on DMNA decomposition on either the ground state or the excited electronic state indicate that a number of unresolved issues clearly exist between the nitro−nitrite isomerization and NO_2 elimination mechanisms for the initial steps in the decomposition of DMNA. For a sensible comparison of these well dispersed and often confusing results on DMNA decomposition, all the various experimental conditions also need to be kept in mind. For a brief review, different plausible decomposition channels of DMNA are presented in Figure 1.

Theoretical Section. To date, ground state DMNA decomposition has been studied theoretically mostly by Thompson and co-workers.[16] To the best of our knowledge, excited electronic state decomposition of DMNA has yet not been studied theoretically. To explain experimental results for both ground state and excited electronic state decomposition of DMNA, often computational work has been focused on the structurally related compound, nitramide (H_2NNO_2), because of its reduced number of heavy atoms and simplicity for computation.[17−20]

The major discrepancies found among different experimental results on the DMNA decomposition are primarily concerned with two mechanisms: NO_2 elimination and nitro−nitrite isomerization. Therefore, all the theoretical results concerning these two channels are summarized below either for H_2NNO_2 or DMNA depending on the availability of the results in the literature. The nitro−nitrite isomerization activation barrier with the important geometrical parameters for the transition state and the $N-NO_2$ bond dissociation energy predicted for H_2NNO_2 and DMNA are summarized in Table 1.

Saxon et al.[17] and Seminario et al.[18] investigated ground state nitro−nitrite isomerization and NO_2 elimination channels of H_2NNO_2 at the MRCISD/6-31G(d)//MCSCF/4-31G and nonlocal density functional theories, respectively. Both of them conclude that the nitro−nitrite isomerization and the NO_2 elimination channels would be competitive in the ground

- Initial elimination of O with formation of nitrosamine:

  Major channel, solid DMNA at room temperature, photolysis at 253.7 nm.

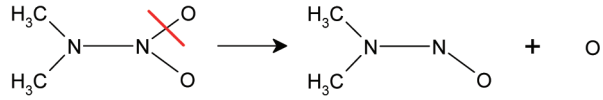

- Nitro-nitrite isomerization:

  Minor (40%) channel, room temperature gaseous DMNA, thermolysis at 900 K.

  Major (96%) channel, molecular beam, photolysis at 226 and 193 nm.

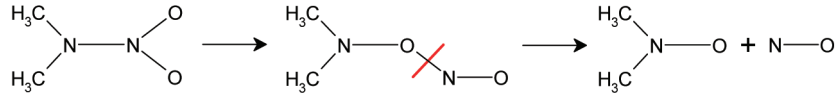

- NO_2 elimination:

  Major channel, room temperature gaseous DMNA, thermolysis at 900 K, 1060-1250 K, 466-525 K.

  Major channel, room temperature gaseous DMNA, photolysis at 266 and 248 nm.

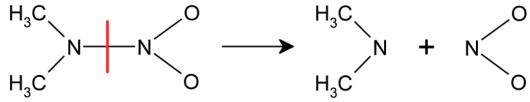

- HONO elimination:

  Minor (3%) channel, room temperature gaseous DMNA, photolysis at 248 nm.

  Minor (4%) channel, molecular beam, photolysis at 226 nm.

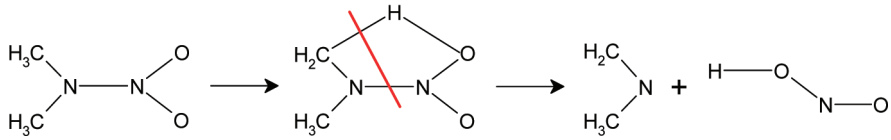

Figure 1. Different decomposition channels observed for DMNA with different experimental conditions.

electronic state of H_2NNO_2. As shown in Table 1, the transition states (TS) reported by both Saxon et al.[17] and Seminaro et al.[18] have loose geometries with long N1−N2 (∼2.8 Å) and N1−O1 (∼3.2 Å) distances.

Soto et al.[20a] also investigate the nitro−nitrite isomerization and N−NO_2 bond dissociation channels for H_2NNO_2 at the CASPT2(14,11)/ANO-L level of theory and obtain a loose nitro−nitrite isomerization TS geometry: the N1O1 bond distance is 2.64 Å, and the N1O2 bond distance is 2.0 Å. Employing B3LYP/6-311G(d,p) level of theory Thompson and co-workers[16a] also concludes that the nitro−nitrite isomerization of DMNA occurs through a loose TS geometry and NO_2 elimination is predicted to be the main decomposition channel of gas phase DMNA in the ground state.

Morokuma and co-workers,[19] in contrast, find only a tight TS geometry in the ground state of H_2NNO_2 at the MP2/6-311G(d,p) and QCISD(T)/6-311G(d,p) levels of theory: the N1−N2 distance is ∼2.43 Å and N1−O1 only ∼1.32 Å. The activation energy at QCISD(T)/6-311G(d,p) level is calculated to be 29.7 kcal/mol, significantly lower than the barrier height predicted by Saxon et al.[17] and Seminaro et al.[18] Accordingly, they conclude that a loose nitro−nitrite isomerization TS does not exist in the ground electronic state for H_2NNO_2. They also conclude that the nitro−nitrite isomerization would prevail over the NO_2 elimination at least at lower temperature because at the G2 level of theory the nitro−nitrite isomerization TS activation energy barrier is predicted to be 20.8 kcal/mol below the N−NO_2 bond dissociation energy. Note that this explanation is in contrast with the experimental observation of DMNA decomposition at low temperature.[9,10]

With regard to investigation of excited electronic state decomposition of nitramine, Soto and co-workers[20b] use the CASPT2(14,11)/ANO-L level of theory and find that the N−NO_2 bond dissociation energy for H_2NNO_2 on its S_1, S_2, and S_3 surfaces are 21.4, 5.1, and 6.2 kcal/mol, respectively. From computed potential energy curves leading to adiabatic NO_2 elimination for H_2NNO_2 in the excited electronic states, they conclude that if NO_2 elimination takes place in the excited electronic state decomposition NO_2 can only be generated in its ground X^2A_1 or excited $A1^2B_2$ electronic state. This result is in good agreement with the experimental results obtained by Sausa and co-workers[12] and Stephenson and co-workers.[13] In their computation, Soto et al.,[20b] however, did not focus on whether a nitro−nitrite isomerization channel is accessible in the upper excited electronic states for this compound.

Thus, the available theoretical results on decomposition of DMNA or related compounds in either the ground or excited electronic states indicate that some disagreements exist concerning the activation energy barrier and the nature of the TS associated with the nitro−nitrite isomerization. To resolve these

TABLE 1: Optimized Geometries (Bond Lengths in Ångstroms) for the Transition State of the Nitro−Nitrite Isomerization of NH_2NO_2/$(CH_3)_2NNO_2$/CH_3NHNO_2 in the Ground Electronic State

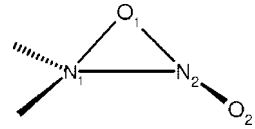

compounds	nature of TS	level of theory	bond lengths	activation barrier (kcal/mol)[a]	ref
H_2NNO_2	loose	DFT-GGA/DZVPP	N1−N2 = 2.831 N1−O1 = 3.193	48.7 (48.4)	18
	loose	MCSCF/4-31G	N1−N2 = 2.845 N1−O1 = 3.214	40.7 (40.55)	17
	tight	MP2/6-311G(d,p)	N1−N2 = 2.428 N1−O1 = 1.319		19
		QCISD(T)/6-311G(d,p)	N1−N2 = 2.368 N1−O1 = 1.119	29.7 (44.7)	
	loose	CASPT2(14,11)/ANO-L	N1−N2 = 2.64 N1−O1 = 2.00	63.55 (53.69)	20
$CH_3(H)NNO_2$	loose	B3LYP/6-311+G(d)	N1−N2 = 2.618 N1−O1 = 2.644	51.84 (44.64)	21
$(CH_3)_2NNO_2$	loose	B3LYP/6-311G(d,p)	N1−O1 = 2.708 N1−O2 = 2.408	52.6 (39.9)	16a
	tight	MP2/6-31G(d)	N1−N2 = 1.90 N1−O1 = 2.00	94.0 (40.0)	present result
	loose	MP2/6-31G(d)	N1−N2 = 2.80 N1−O1 = 2.30	69.0	
	loose	CASSCF(10,7)/6-31G(d)		57.0 (30.0)	

[a] Numbers within brackets give the calculated N−NO_2 bond dissociation energies (kcal/mol).

issues, further computation on DMNA decomposition is needed at a suitable level of theory that can provide a balanced treatment of the various dissociation channels at different excitation wavelengths and within different excited states for this system.

III. Experimental Procedures

The experimental setup consists of ns laser systems, a supersonic jet expansion pulsed nozzle, and two vacuum chambers: a time-of-flight mass spectrometer chamber and a LIF chamber, described in detail elsewhere.[22] For the nanosecond laser experiments, a single pump/probe laser beam at 226 nm is used both to initiate dissociation of DMNA and detect the NO product following a one color (1 + 1) resonance-enhanced two-photon ionization (R2PI) scheme [$A^2\Sigma^+(v'=0) \leftarrow X^2\prod(v''=0)$ and I ← A transitions] through TOFMS. The UV laser wavelengths used in the nanosecond laser experiments are generated by a pulsed dye laser, pumped by the second harmonic (532 nm) of a Nd:YAG laser's fundamental output (1.064 μm), in conjunction with a nonlinear wavelength extension system. Typical pulse energy of the UV laser is ∼16−300 μJ/pulse, which gives a laser beam intensity (I) of $\sim 6.5 \times 10^6 - 1.2 \times 10^8$ W/cm^2 for an 8 ns pulse duration at a focused beam diameter of 0.2 mm. For the detection of an OH product from DMNA through LIF, a UV laser at 226 nm is used to initiate the dissociation of the parent molecules, and one additional laser (308 nm) is required to excite the OH $A^2\Sigma^+(v'=0) \leftarrow X^2\prod(v''=0)$ transition. Detection of the OH product from DMNA has been calibrated by the observation of the OH radical generated by photolysis of nitric acid (HNO_3) at 193 nm inside a quartz capillary attached to the pulse nozzle.

Photolysis of DMNA is also performed inside a quartz capillary attached to the pulsed nozzle by both 193 and 226 nm radiation, and subsequently products are detected in time-of-flight mass spectrometer by 118 nm ionization. An ArF excimer laser is used to generate radiation at 193 nm, and the ninth harmonic (118 nm) of a seeded Nd:YAG laser is generated in a 1:10 mixture of Xe/Ar at 330 Torr pressure previously discussed elsewhere.[23]

Isolated gas phase DMNA molecules are generated through a supersonic jet expansion. The nozzle employed for the sample beam generation is constructed from a Jordan Co. pulsed valve. DMNA is heated to about 350 K in a glass vial outside the nozzle and brought into the molecular beam by helium carrier gas at 30 psig backing pressure.

The experiment is run at a repetition rate of 10 Hz. The timing sequence for the pulsed nozzle, ablation laser, and ionization laser is controlled by a time delay generator (SRS DG535). The molecular beam is perpendicularly crossed by a UV laser beam that is focused to a spot size of about 0.2 mm at the ionization region of a time-of-flight mass spectrometer. A background pressure of 1×10^{-5} Torr is maintained in the vacuum chamber during the experiment. Ions are detected by a microchannel plate detector (MCP) and fluorescence is detected by a photomultiplier tube (PMT). Signals are recorded and processed on a PC using a box car averager (SRS SR 250) and an ADC card (Analog Devices RTI-800).

IV. Theoretical Procedures

All geometry optimizations relevant to excited electronic sate decomposition of DMNA are executed at the CASSCF/6-31G(d) level of theory and with the Gaussian 03 program.[24] In addition, geometry optimizations relevant to ground electronic state decomposition of DMNA are performed at both the MP2 and CASSCF levels of theory with both 6-31(d) and 6-311G(d,p) basis sets. No symmetry restrictions are applied during the calculations. To explore the excited state potential energy surfaces, the active space comprises 14 electrons distributed in 11 orbitals, denoted as CASSCF(14,11) (see Figure 2). Orbitals used in the active space are one N nonbonding $2S_N$ orbital, two NO bonding orbitals σ_{NO}, two NO antibonding orbitals σ_{NO}*, one delocalized ONO π-bonding orbital π_{ONO}, one delocalized ONO π-antibonding orbital π_{ONO}*, one bonding NN orbital σ_{NN},

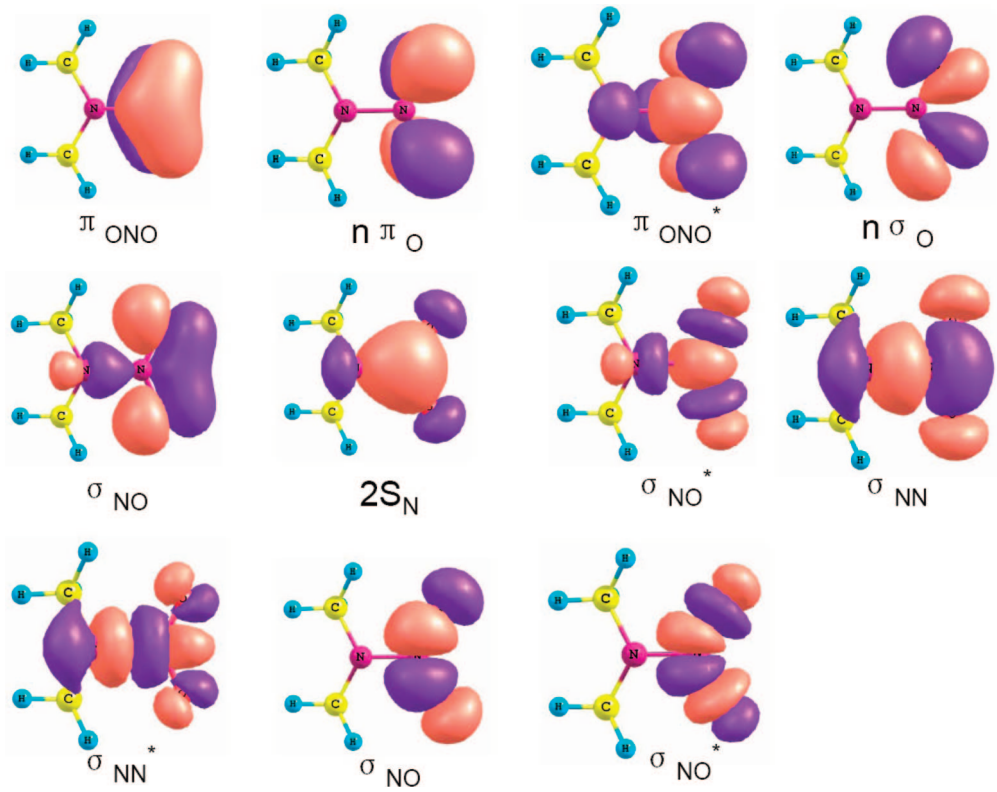

Figure 2. Orbitals used in the active space for CASSCF calculations for DMNA. These orbitals thus comprise the full active space (14,11) for DMNA (14 electron in 11 active orbitals).

one NN antibonding σ_{NN}*, one π-nonbonding orbital nπ_O, and one σ nonbonding nσ_O, as illustrated in Figure 2. The same active space was previously used by Soto et al.[20] for computations for NH_2NO_2. To avoid convergence failure problems, a reduced (10,7) active space is also used for the excited state calculations. Vertical excitation energies are calculated by state averaging over the ground and excited states with equal weights for each state. Critical points (minima and transition state structures) are characterized by analytical frequency calculations, and minimum energy paths are calculated using an intrinsic reaction coordinate (IRC) algorithm implemented in the Gaussian 03. As the present Gaussian code cannot perform analytical frequency calculations using more than eight orbitals in the active space,[24] frequency calculations and IRC calculations, which require initial force constants, are performed using a reduced active space (10,7) with the same basis set.

V. Experimental Results and Discussion

The PF/FD technique[25] has been employed in the investigation of the excited electronic state decomposition of DMNA. In our PF/FD experiments, DMNA is excited to an excited electronic state by absorption of a single UV photon at different excitation wavelengths (226 and 193 nm), and then it decomposes into products through certain decomposition pathways. The dissociation products are subsequently detected either by the same laser or a different, time delayed laser, either in TOFMS or by LIF spectroscopy.

Nitric oxide (NO) is observed as a major decomposition product from the photodissociation of DMNA at 226 nm in TOFMS. This result was also previously obtained by Sausa and co-workers.[14] The 226 nm excitation wavelength also corresponds to the resonance (0−0) vibronic band of the $A^2\Sigma^+ \leftarrow X^2\prod$ electronic transition of the NO product. Therefore, by scanning this laser excitation wavelength, a (1 + 1) R2PI rotationally resolved spectrum of the NO product from DMNA is obtained. Note that the DMNA absorption near the excitation wavelength is smooth, structureless, and essentially constant. In addition, a few comments can be made to clarify that the NO product is generated from the excited electronic state decomposition of DMNA following single photon absorption based on the line width of the NO mass peak. Additional kinetic energy from photofragmentation following two-photon absorption should generate additional line width for fragment mass channels. Moreover, if DMNA absorbs two photons at 226 nm sequentially, it can be fragmented into NO following ionization. This will also lead to broadening of the line width of the NO mass signal. Experimentally, the line width of the NO mass channel is observed to be about 10 ns, which is the instrumental line width of our laser/TOFMS set up. Therefore, we believe that the NO product is associated with a single photon absorption by DMNA.

Photolysis of DMNA can produce several possible primary intermediates in the initial step of photodissociation, which can finally render the NO product. These include NO_2, HONO, dimethylaminonitrite after nitro−nitrite isomerization, and dimethylnitrosamine after elimination of an O atom. Each intermediate corresponds to a different possible decomposition channel of DMNA as is illustrated in Figure 1. Therefore, detection of the NO product from the photodissociation of DMNA is not an unambiguous identification of any of the four possible decomposition channels of DMNA. To exclude some of these possibilities, different nanosecond laser experiments are performed, which are presented and contrasted below.

NO_2 Elimination. To justify whether NO_2 is an intermediate precursor of the NO product in the excited electronic state decomposition of DMNA, investigation of the decomposition of several other nitro-containing compounds such as NO_2 gas and nitromethane is undertaken. NO_2 gas renders NO product

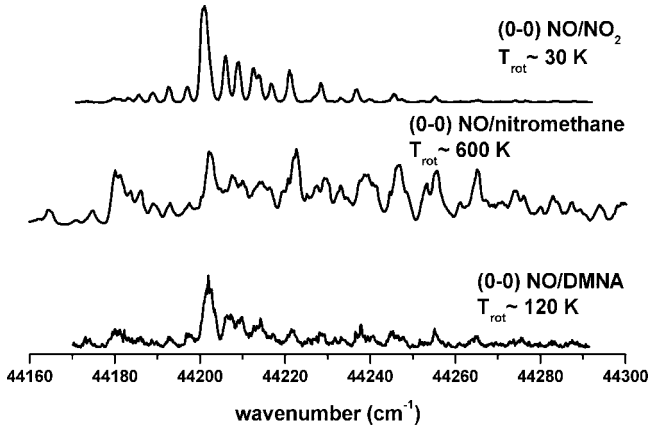

Figure 3. One color (1 + 1) R2PI spectra of the vibronic transitions [$A^2\Sigma^+(v'=0) \leftarrow X^2\prod(v''=0)$] of the NO product from the excited electronic state decomposition of DMNA and other nitro-containing molecules (nitromethane and NO_2 gas). Rotational temperature simulations with Boltzmann distribution show that NO from NO_2 gas, nitromethane, and DMNA generates rotational temperatures of 30, 600, and 120 K, respectively.

due to photodecomposition. Nitromethane, on the other hand, is well known to produce the NO product through an NO_2 intermediate.[26] Therefore, comparison of the rotational and the vibrational distributions of the NO product obtained from photolysis of these nitro-containing compounds to that from photolysis of DMNA is expected to serve as a guide to determine whether NO_2 is a potential and appropriate intermediate in the excited electronic state decomposition of DMNA.

(1 + 1) R2PI spectra of NO from photolysis of DMNA, and other nitro-containing compounds, in the NO $A^2\Sigma^+(v'=0) \leftarrow X^2\prod(v''=0)$ transition region are presented and contrasted in Figure 3. All the spectra are obtained under similar experimental conditions such as laser energy (50 μJ/pulse), backing pressure (30 psig), collisionless molecular beam conditions, etc. The most intense band centered at 44202 cm^{-1} in these spectra is assigned to the (Q_{11}+P_{21}) band head[27] of the $A^2\Sigma^+(v'=0) \leftarrow X^2\prod(v''=0)$ transition of NO. Comparison of simulated spectra based on Boltzman population distribution of the NO rotational energy levels at the $v''=0$ state to the R2PI spectra of the NO product from DMNA, NO_2, and nitromethane generates rotational temperatures of 120, 30, and 600 K, respectively.

Photodissociation of nitromethane at 226 nm excitation renders NO product through an NO_2 intermediate.[26] NO from nitromethane is rotationally hotter (600 K) than that from NO_2 gas and has a vibrational distribution similar to that from NO_2 gas, as both (0−0) and (0−1) transitions are observed. Therefore, if NO_2 is an intermediate of the excited electronic state decomposition of DMNA, the NO product from DMNA through the NO_2 precursor is also expected to have similar or hotter rotational and vibrational distributions than that of NO from NO_2 gas. If NO_2 is an intermediate in the decomposition of DMNA, the final NO product should not have rotational or vibrational distributions colder than that from NO_2 gas.

Nonetheless, on the contrary, NO from DMNA at 226 nm photoexcitation is vibrationally colder (only the (0−0) transition is observed) than that from NO_2 gas (both (0−0) and (0−1) transitions are observed), and NO from DMNA (226 nm) is rotationally hotter (120 K) than that from NO_2 gas. These differences indicate that NO_2 can not be an intermediate precursor of the NO product in the excited electronic state decomposition of DMNA. This observation is, in principle, direct evidence for the exclusion of NO_2 elimination as a major

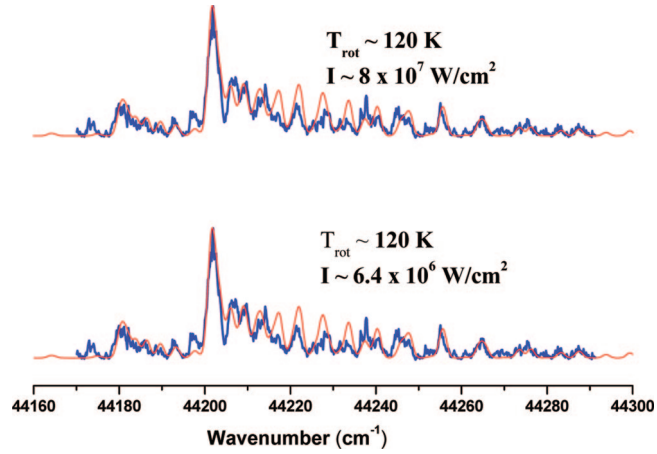

Figure 4. Comparison of the one color (1 + 1) R2PI spectra of the vibronic transitions [$A^2\Sigma^+(v'=0) \leftarrow X^2\prod(v''=0)$] of the NO product from excited electronic state decomposition of DMNA at different laser intensities (W/cm^2).

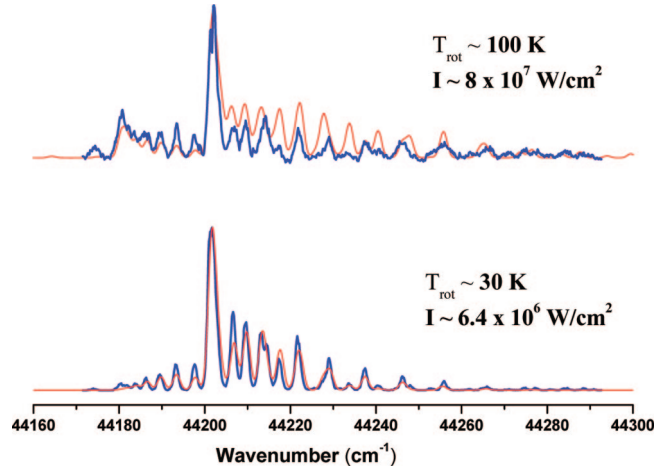

Figure 5. Comparison of the one color (1 + 1) R2PI spectra of the vibronic transitions [$A^2\Sigma^+(v'=0) \leftarrow X^2\prod(v''=0)$] of the NO product from the excited electronic state decomposition of 0.001% NO_2 at different laser intensities (W/cm^2).

excited electronic state decomposition mechanism of DMNA. Nonetheless, one can argue that the reason for not observing the (0−1) transition of the NO product from photodecomposition of DMNA may be due to the extremely low concentration of NO_2 generated in the excited electronic state decomposition of DMNA. Therefore, to obtain an unambiguous corroboration of the fact that NO_2 is not an intermediate in the excited electronic state decomposition of DMNA, laser intensity dependence of NO spectra from DMNA and NO_2 gas is explored and contrasted below.

The (1 + 1) R2PI spectra of NO from photodissociation of DMNA in the NO $A^2\Sigma^+(v'=0) \leftarrow X^2\prod(v''=0)$ transition region for two different laser intensities are presented in Figure 4. Both spectra are rotationally well resolved and show similar patterns, which produces similar rotational temperature (~120 K). This necessitates the conclusion that rotational temperature (in other words, R2PI spectra) of the NO product from photodissociation of DMNA at 226 nm excitation is laser intensity independent.

Similar (1 + 1) R2PI spectra of the NO product from photodissociation of 0.001% NO_2 seeded in He carrier gas in the same NO $A^2\Sigma^+(v'=0) \leftarrow X^2\prod(v''=0)$ transition region for two different laser intensities are presented in Figure 5. These spectra clearly show different spectral patterns at different laser

intensities. At low (6.4×10^6 W/cm^2) laser intensity, a rotational temperature of about 30 K is observed, much colder than that produced at high laser intensity (8×10^7 W/cm^2), which is about 100 K. This behavior indicates that rotational temperature of the NO product from photodissociation of NO_2 at 226 nm excitation is laser intensity dependent.

Photodissociation of NO_2 in this region with different laser intensities using a similar PF/FD technique was previously investigated by Im et al.[28a] Although photodissociation of NO_2 near 226 nm could be studied very efficiently by probing the entire energy distribution of the fragments using the velocity map imaging technique,[28b] Im et al. probed only rotational and vibrational distributions of the NO product from NO_2 using TOFMS and unambiguously determined internal temperatures by comparing the experimental REMPI spectrum of NO with the simulated one. They concluded that single photon dissociation of NO_2 through the 2^2B_2 state at 226 nm photoexcitation with low laser intensity renders a rotationally cold (~30 K) NO product. Multiphoton dissociation obtained at high laser intensity, on the other hand, takes place through either a Rydberg excited state or an ion-pair state producing rotationally hot (~100 K) NO product. If photodissociation of DMNA at 226 nm excitation renders the primary decomposition product NO_2 in the ground state, one would expect to observe similar laser intensity dependence of the NO rotational temperature. Instead, absence of this behavior in the decomposition of DMNA at 226 nm excitation corroborates the fact that ground state NO_2 is not an intermediate in the decomposition of DMNA.

To probe the formation of excited state NO_2 photoproduct, LIF and emission spectroscopy are performed. If NO_2 is the primary photodecomposition product of DMNA and is generated in an excited state (either 1^2B_2 or 2^2B_1), one would expect to observe fluorescence emission from the excited state NO_2 following the photolysis of DMNA at 226 nm. The radiative lifetime for these transitions of NO_2 in the visible region is very long, typically ~30−120 μs,[29] indicative of a small transition oscillator strength. Radiative lifetime of NO for the transition from $A^2\Sigma^+$ state to ground state in the UV region is significantly shorter (~200 ns)[30] than that of NO_2 excited states in the visible region. Therefore, both fluorescences can easily be distinguished in LIF or emission spectroscopy. Upon photolysis of DMNA at 226 nm no emission is observed from an excited state of NO_2. Instead, NO LIF signal with ~200 ns (fwhm) radiative lifetime is observed when the photolysis laser is tuned to the resonance position of the NO (0−0) transition. The LIF spectrum of NO in this region from photodissociation of DMNA, given in Figure 6a, displays a hot rotational temperature of ~120 K.

Fluorescence emission with ~35 μs lifetime from the excited state of NO_2 product following the photodissociation of nitromethane (CH_3NO_2) at 193 nm was previously observed by Butler et al. using product emission spectroscopy.[31] By means of translational energy distribution of products, they concluded that the primary decomposition channel of CH_3NO_2 at 193 nm renders the vibrationally hot 1^2B_2 excited electronic state of NO_2. A similar attempt is also made by us to repeat the decomposition of nitromethane and DMNA at 193 nm. We observe fluorescence emission in the visible region with a long lifetime (~4 μs) following nitromethane photodissociation (see Figure S1 of Supporting Information). No emission (NO or NO_2) is observed following DMNA photodissociation at 193 nm.

Therefore, results obtained in resonance enhanced two photon ionization spectroscopy, and fluorescence emission spectroscopy for detection of the NO_2 product corroborate the fact that neither ground state (X^2A_1) nor excited state (1^2B_1 or 1^2B_2) NO_2 is a primary photodecomposition product of DMNA at 226 and 193 nm excitations.

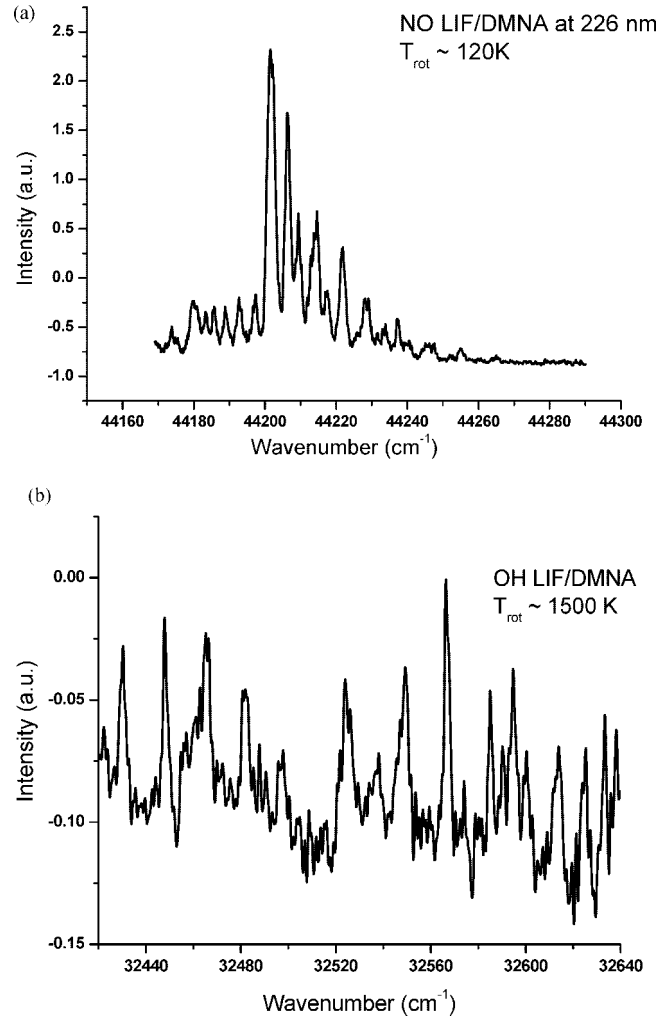

Figure 6. LIF spectrum of (a) NO near 226 nm and (b) OH near 308 nm from excited electronic state decomposition of DMNA at 226 nm.

HONO Elimination. To assess whether HONO is an intermediate precursor of NO in the excited electronic state decomposition of DMNA, experimental detection of the OH radical is undertaken. If HONO is a precursor of product NO, decomposition of DMNA should produce equimolar quantities of OH and NO radicals. As OH has a high ionization energy (IE = 13.5 eV), detection of OH is not performed using TOFMS. Instead, LIF spectroscopy is used to detect the OH radical from photodecomposition of DMNA. To detect the OH product from photolysis of DMNA by LIF spectroscopy, two lasers are required: one laser at 226 nm is used to initiate dissociation of the parent molecule, and another at 308 nm is used to excite OH, corresponding to the (0−0) band of its $A^2\Sigma^+ \leftarrow X^2\prod$ electronic transition. Note that DMNA does not have any absorption at 308 nm,[36] and therefore, 308 nm does not contribute to the dissociation process of DMNA.

The LIF spectrum of OH from photolysis of DMNA at 226 nm is shown in Figure 6b. OH is found to have a very hot (~1500 K) rotational distribution when the excitation laser (308 nm) is tuned to the resonance position of the OH (0−0) transition. Photodecomposition of DMNA at 226 nm generates less than 1.5 mV of OH LIF signal at the maximum gain of the photomultiplier tube (PMT), when OH signal intensity is fully

optimized by overlapping both 226 and 308 nm beams with above absorption saturation energies. Under similar experimental conditions, the maximum LIF signal intensity of the NO product from photodissociation of DMNA at 226 nm is observed to be 50 mV when the photolysis laser is tuned to the resonance position of the NO (0−0) transition. These maximum LIF signal intensities of NO and OH can be compared to evaluate the yield ratio between these two products.

To estimate the yield ratio between the NO and the OH products in the excited electronic state decomposition of DMNA, however, one must relate the maximum LIF signal intensities of NO and OH to the population of the individual rotational states responsible for the transition at 120 and 1500 K, respectively. For a Boltzmann distribution for which $kT \gg 2B(J+1)$, the ratio of the population at a certain rotational J level to the entire population is given by[32]

$$\frac{N_j}{N_o} = \left(\frac{hcB}{kT}\right)(2J + 1)\exp\left[\frac{-BJ(J+1)hc}{kT}\right] \quad (1)$$

in which h is Planck's constant, c is the speed of light, k is Boltzmann's constant, and B (in cm^{-1}) is the rotational constant. This equation can determine what fraction of the entire population contributes to the maximum LIF signal intensity at a certain temperature. Another important parameter is the Franck−Condon (FC) factor for an electronic transition, which also contributes to the maximum LIF signal intensity of a particular species.

Thus, by comparison of the maximum LIF signal intensities of NO and OH radicals along with their respective FC factors of the (0−0) transition and the population of rotational states responsible for the transition, the yield ratio between the NO and the OH products is calculated to be 1:0.04. The branching ratio could be determined more accurately by including the differences of the absorption line width between NO and OH species, which depend on their translational temperatures. Nonetheless, the NO absorption frequency is 44274 cm^{-1} (226 nm), which is greater than the OH absorption frequency of 32467 cm^{-1} (308 nm). Thus, the possible greater temperature to mass ratio for the OH radical can be balanced by the greater absorption frequency for the NO molecule. This implies that the absorption line width difference between NO and OH may be small. Therefore, the final influence from the absorption line width difference can be reasonably ignored because the branching ratio will not be significantly changed even if it is included in the calculation. In fact, our estimation including only rotational Boltzmann distributions and FC factor calibration shows 4% branching ratio for the HONO elimination channel, which is in good agreement with that of 3% reported in previous work.[12] The large discrepancy between the OH and NO yields indicates that the HONO elimination channel has only a minor contribution to the overall excited electronic state decomposition of DMNA.

Nitro−Nitrite Isomerization. Experimental justification of nitro−nitrite isomerization as a potential excited electronic state decomposition pathway of DMNA is rather complicated in nature. If nitro−nitrite isomerization takes place, one would expect to detect the $(CH_3)_2NO$ radical which is generated by nitro−nitrite isomerization followed by rapid O−NO bond scission; however, $(CH_3)_2NO$ is not observed in TOFMS employing 118 nm ionization. Two reasons for not observing $(CH_3)_2NO$ in the TOFMS can be mentioned: $(CH_3)_2NO$ neutral or cation might be unstable and the IP of $(CH_3)_2NO$ might be above 10.5 eV. To the best of our knowledge, the IP of $(CH_3)_2NO$ is not reported in the literature. Collisions on the other hand can stabilize the radical yielding $(CH_3)_2NOH$ (61 amu), which is a well-known stable compound with low IP (9.2 eV). Therefore, in order to explore the nitro−nitrite isomerization channel, photolysis experiments at 193 and 226 nm are performed inside a quartz capillary attached to the pulsed nozzle.

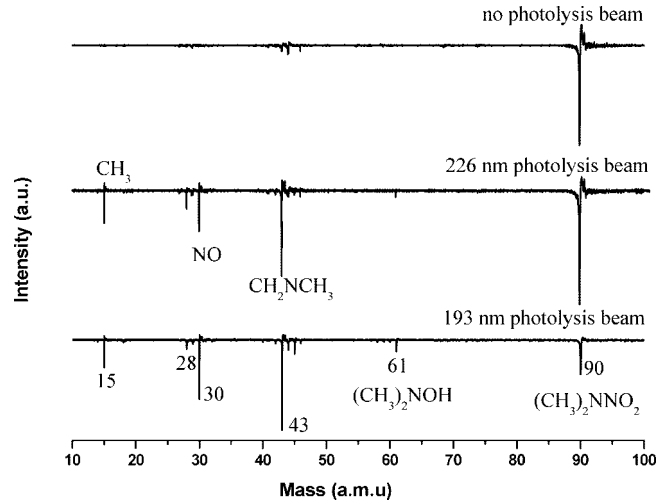

Figure 7. TOFMS obtained at three different conditions: (1) photolysis of DMNA at 193 nm inside quartz capillary and subsequent product detection by 118 nm ionization (bottom), (2) photolysis of DMNA at 226 nm inside quartz capillary and subsequent product detection by 118 nm ionization (middle), (3) photolysis beam is blocked (top).

The TOFMS, which are obtained when gaseous DMNA seeded in He carrier gas is photolyzed inside a quartz capillary using 193 or 226 nm radiation with products subsequently detected by 118 nm ionization in TOFMS, are presented in Figure 7. The photolysis of DMNA at both 193 and 226 nm renders the same mass distribution of products indicating that the photodecomposition behavior of DMNA does not change at these two different excitation wavelengths.

Direct observation of 61 amu mass channel ($(CH_3)_2NOH$) in the time of fight mass spectrometer necessitates the conclusion that the rapidly produced NO arises from the nitro−nitrite isomerization mechanism, followed by extremely rapid scission of the very weak O-NO bond

$$(CH_3)_2NNO_2 \rightarrow (CH_3)_2NONO \rightarrow (CH_3)_2NO + NO \quad (2)$$

The $(CH_3)_2NO$ radical abstracts one hydrogen atom under high collisional conditions, producing the $(CH_3)_2NOH$ product. This $(CH_3)_2NOH$ mostly further decomposes to CH_2NCH_3 and H_2O products, providing a very prominent mass peak at mass channel 43 amu (CH_2NCH_3)

$$(CH_3)_2NO + H \rightarrow (CH_3)_2NOH \rightarrow CH_2NCH_3 + H_2O \quad (3)$$

Observation of mass channel 61 amu is direct experimental evidence for the nitro−nitrite isomerization channel in the excited electronic state decomposition of DMNA; nonetheless, it does not address the inter- or intramolecular nature of the nitro−nitrite isomerization. DMNA decomposition inside the quartz capillary happens under highly collisional conditions. At room temperature (300 K), using 40 psig backing pressure, the collision frequency is calculated to be 3.4×10^{10} s^{-1} for only He carrier gas inside the quartz capillary (ca. 2800 Torr pressure). This provides a mean collision time (average time between two successive collisions) of 29 ps. The laser pulse duration (8 ns) is longer than the mean collision time. Therefore, further photodecomposition of the products obtained from unimolecular decomposition of DMAN is also possible while

the products are undergoing several collisions. As a result, if NO_2 elimination is the primary initial photochemical process in the unimolecular decomposition of DMNA at 193 and 226 nm, one would expect several collisional recombination products under these highly collisional conditions. These products could include $(CH_3)_2NONO$ (after collisional recombination of NO_2 with $(CH_3)_2N$) and $(CH_3)_2NNO$ (after collisional recombination of NO with $(CH_3)_2N$).

$(CH_3)_2NNO$ is a very stable compound with ionization energy of 9.5 eV. This is expected to be detected by 118-nm ionization; however, no signal at 74 amu ($(CH_3)_2NNO$) is observed. Instead, the only collisional product observed is $(CH_3)_2NOH$. In addition, we have already established the fact that neither ground state NO_2 nor excited state NO_2 is an excited electronic state decomposition product of DMNA. This result excludes the possibility of the intermolecular nature of nitro−nitrite isomerization by collisional recombination of NO_2 after initial NO_2 elimination; rather, a nitro−nitrite isomerization takes place through an intramolecular isomerization pathway.

Therefore, the above experimental results on the excited electronic state decomposition of DMNA necessitate the conclusion that a nitro−nitrite isomerization is the primary decomposition channel of DMNA from excited electronic states with a minor contribution from an HONO elimination mechanism. The approximate branching ratio between nitro−nitrite isomerization and HONO elimination channels is estimated to be 1:0.04. NO_2 elimination is not the excited electronic state decomposition mechanism of DMNA. Although similar nitro−nitrite isomerization mechanisms have been reported for the ground state decomposition of nitroalkanes and nitroaromatics, and even for DMNA, present experimental results are not consistent with the previous experimental reports,[12−14] which suggest that excited electronic state decomposition of DMNA proceeds mostly through NO_2 elimination.

Both previous experiments on the photodecomposition of gaseous DMNA at 266[13] and 248 nm[12] are done in a cell at room temperature under almost collisionless conditions. Our experiments are done under molecular beam conditions. We used 236 and 248 nm photolysis to photodissociate DMNA in the molecular beam; however, we did not observe any product. Therefore, experimentally we do not have an obvious immediate rationalization that can address the unresolved issues of NO_2 elimination and nitro−nitrite isomerization mechanisms in the excited electronic state decomposition of DMNA. To make some comment and bring these different experimental results, obtained under somewhat different experimental conditions (e.g., temperature, pressure, etc.) into harmony, detailed theoretical computation is pursued to explore the nitro−nitrite isomerization and NO_2 elimination channels for DMNA decomposition. We point out in the General Conclusions section below, by combining both experimental and theoretical results, that the apparent disagreements between experimental results on DMNA decomposition arise due to different experimental conditions, in particular temperature in this instance.

VI. Theoretical Results and Discussion

The major discrepancies found among different experimental results on both thermal and excited electronic state decomposition of DMNA are primarily concerned with two mechanisms: NO_2 elimination and nitro−nitrite isomerization. Therefore, we consider below the theoretical exploration of these two channels in order to judge which of them is energetically more favorable. We shall start with ground state calculations on DMNA decomposition because, they not only improve understanding

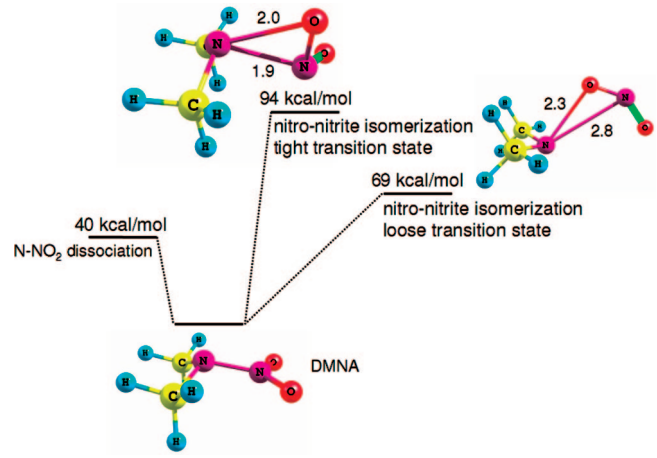

Figure 8. Both tight and loose TS geometries for the DMNA nitro−nitrite isomerization optimized at the MP2/6-31G(d) level of theory for the ground electronic state. Relative activation energies are given and can be compared to the $N-NO_2$ bond dissociation energy computed at the same level of theory.

of excited electronic state decomposition behavior of DMNA but they also justify the level of theory by establishing agreement between experimental and theoretical results. Moreover, we shall see shortly that, because of the presence of a conical intersection, ground and excited electronic state decomposition pathways are highly correlated along the nitro−nitrite isomerization reaction coordinate. These results and understandings are necessary and essential for providing new insight into the overall decomposition mechanism and dynamics of DMNA.

Ground Electronic State Decomposition. The nitro−nitrite isomerization followed by extremely weak NO−NO bond scission is a thermochemically allowed decomposition mechanism of DMNA in the ground electronic state. The nature of the TS associated with the nitro−nitrite isomerization channel is a subject of more discussion. Both tight and loose TS geometries are reported in the literature for the nitro−nitrite isomerization in the ground state (see Table 1). A tight TS geometry corresponds to an isomerization for which rotation of NO_2 is substantial at short N−N bond length. A loose TS geometry, on the other hand, corresponds to an isomerization for which rotation of NO_2 does not happen until the N−N bond is elongated substantially. The nitro−nitrite isomerization activation barriers, along with important geometrical parameters and $N-NO_2$ bond dissociation energies estimated by different groups for DMNA and H_2NNO_2, are summarized in Table 1. Note that localization of both tight and loose transition states for either DMNA or NH_2NO_2 at the same level of theory has not been possible.

In contrast, we are able to localize both tight (with a short N−N bond distance) and loose (with a long N−N bond distance) TSs on the ground electronic state surface of DMNA at the MP2/6-31G(d) level of theory, as shown in Figure 8. In the tight transition state, the N1N2 bond distance is predicted to be 1.9 Å, and N1O1 is predicted to be 2.0 Å (see Figure 8). The activation energy at the MP2/6-31G(d) level is calculated to be 94 kcal/mol. In the loose transition state geometry, the N1N2 bond distance is predicted to be 2.8 Å, and the N1O1 bond distance is predicted to be 2.3 Å (see Figure 8). The activation energy barrier of the loose TS is calculated to be 69 kcal/mol, significantly lower in energy than that of tight TS at the MP2/6-31G(d) level.

In spite of an exhaustive search to reproduce both tight and loose TS geometries for the ground electronic state at the

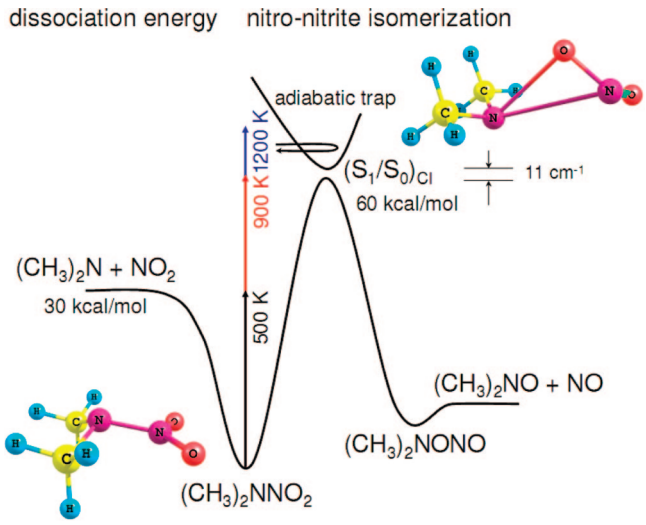

Figure 9. A schematic diagram of the N−NO_2 bond dissociation and nitro−nitrite isomerization pathways presented along two different directions with their respective energies of dissociation and activation computed at CASSCF(10,7)/6-31G(d) level of theory. Nitro−nitrite isomerization TS exists near the $(S_1/S_0)_{CI}$ conical intersection, and its energy is calculated to be ∼3 kcal/mol below the energy barrier of the conical intersection. The adiabatic energy gap between the S_1 and S_0 surfaces near $(S_1/S_0)_{CI}$ is calculated to be 11 cm^{-1}.

CASSCF(10,7)/6-31G(d) level of theory, however, only a loose TS geometry for the nitro−nitrite isomerization of DMNA is obtained. In addition, in the neighborhood of the nitro−nitrite tight TS region predicted at the MP2 level, an $(S_1/S_0)_{CI}$ conical intersection is localized at both CASSCF(10,7) and CASSCF(14,11) levels of theory with the 6-31G(d) basis set. The adiabatic energy gap between the S_0 and the S_1 surfaces near the $(S_1/S_0)_{CI}$ conical intersection is computed to be 11 cm^{-1} at the CASSCF(10,7)/6-31G(d) level.

Similar behavior was also found by Soto et al.[20a] for the ground state potential energy surface of structurally related NH_2NO_2 at both CASSCF and CASPT2 levels of theory with an ANO-L basis set. They found that CASSCF and CASPT2 levels of theory could not localize any tight nitro−nitrite TS but could localize a loose nitro−nitrite TS. In addition, near the tight TS region predicted at the MP2 level, they could localize an $(S_1/S_0)_{CI}$ conical intersection. They attributed this discrepancy between multiconfigurational (e.g., CASSF calculation) and monoconfigurational (e.g., HF calculations) methods to the presence of $(S_1/S_0)_{CI}$ conical intersection and concluded that the presence of this conical intersection in the region of the nitro−nitrite isomerization TS repels the S_0 surface down, destroying the tight TS for the nitro−nitrite isomerization.

In accord with Soto et al., we also believe that nitro−nitrite isomerization of DMNA takes place through a loose geometry, which is predicted at the CASSCF(10,7)/6-31G(d) level of theory. In addition, we also believe that the monoconfigurational methods (such as MP2) may overestimate the energy barrier of the tight nitro−nitrite isomerization TS because they cannot judge how the S_0 surface topology can be affected by the proximity of the S_1 surface near the $(S_1/S_0)_{CI}$ conical intersection. Therefore, only the CASSCF level of theory (or MRCI, CASPT2 approaches) will provide the most reasonable theoretical picture of the decomposition of DMNA.

A schematic diagram for the N−NO_2 bond dissociation energy and nitro−nitrite isomerization activation barrier with $(S_1/S_0)_{CI}$ conical intersection of DMNA computed at CASSCF(10,7)/6-31G(d) level is illustrated in the Figure 9. The N−NO_2 bond dissociation energy and the nitro−nitrite isomerization activation barrier are predicted to be 30 and 57 kcal/mol, respectively. The energy barrier for $(S_1/S_0)_{CI}$ conical intersection is predicted to be 60 kcal/mol. Our present computation at the CASSCF(10,7)/6-31G(d) level of theory on the decomposition of DMNA on the ground electronic surface not only predicts the true nature of the TS for nitro−nitrite isomerization but can also explain and integrate all the experimental results for the thermal decomposition of DMNA, as presented in the next three paragraphs.

(a) At relatively low temperature (e.g., ∼500 K) thermolysis, when the system barely reaches the N−NO_2 bond dissociation energy (30 kcal/mol), NO_2 elimination is expected to be the only decomposition mechanism for DMNA. Because of the low vibrational energy excitation ($(3N - 6)RT \approx 29$ kcal/mol) at that temperature, DMNA cannot surmount the activation barrier for the nitro−nitrite isomerization. This has been observed by Lloyd and Fluornoy in their pyrolysis experiment of gaseous DMNA,[9,10] which renders NO_2 elimination as the only decomposition channel for DMNA near 500 K.

(b) At higher temperature (e.g., ∼900 K), when the system can also surmount the activation barrier (57 kcal/mol) of the nitro−nitrite isomerization, both NO_2 elimination and nitro−nitrite isomerization channels are expected to play a role in the overall decomposition mechanism and dynamics for DMNA. The branching ratio between these two channels will depend on many factors, e.g., enthalpy and entropy of the reaction, electronically nonadiabatic transitions, etc. Electronic nonadiabatic effects are indeed important if the coupling between the two interacting adiabatic electronic states is weak enough and the adiabatic energy gap between two electronic states is not large enough near the respective conical intersection. The probability of a nonadiabatic surface jump near a conical intersection depends on the energy gap between the two adiabatic surfaces near that point.[33] If the energy gap (the magnitude of the coupling) between two adiabatic surfaces near the conical intersection point is small enough (weak coupling between the two surfaces), the rate of nonadiabatic transition through this point from one adiabatic surface to another adiabatic surface becomes fast. An illustration of such a consideration was first predicted by Landau and Zener[34] and later has been found in many organic compounds.[35] The adiabatic energy gap between the S_1 and S_0 surfaces near $(S_1/S_0)_{CI}$ is computed to be 11 cm^{-1} (see Figure 9). Therefore, the nitro−nitrite isomerization channel in the ground state can be frustrated due to the presence of the weakly coupled $(S_1/S_0)_{CI}$ conical intersection by transferring some of the ground state populations to the upper electronic surface. Therefore, at high enough temperature, when the system can surmount the nitro−nitrite isomerization activation barrier, NO_2 elimination is still expected to be the major decomposition channel. This has been observed by Golden and co-workers.[8] They observed that only 20% of the total decomposition of DMNA goes through nitro−nitrite isomerization at 900 K.

(c) At even higher temperature (1200 K), an additional important factor, the entropy of the reaction, can also play a role in the overall decomposition mechanism and dynamics for DMNA on the ground potential energy surface. In a chemical reaction if the number of particles in the system increases, entropy of the reaction also increases. Therefore, the NO_2 elimination reaction channel possesses a positive entropy of reaction that becomes a significant factor at higher temperature ($\Delta G = \Delta H - T\Delta S$). This can explain why, for the laser pyrolysis experiments at 900 K, the nitro−nitrite isomerization

TABLE 2: CASSCF(10,7)/6-31G(d) Calculated Vertical Excitation Energies and Relative Energies of the Conical Intersections with Respect to the Energy of FC Geometry, Optimized at the Same Level of Theory

state/CI	configuration	ΔE (eV)
S_1(FC)	(nσ_O,π^*)	4.83
S_2(FC)	(nσ_O,π^*)	5.65
S_3(FC)	(nπ_O,π^*)	6.6
$(S_1/S_0)_{CI}$		2.6
$(S_2/S_1)_X$[a]		4.8
$(S_2/S_1)_{CI}$		4.2

[a] Two S_2/S_1 conical intersections are localized in the S_2 surface, one at shorter N−N bond distance defined as $(S_2/S_1)_X$ and another at longer N−N bond distance defined as $(S_2/S_1)_{CI}$. See text for more details.

represents more than 20% of the total decomposition of DMNA, but in the IRMPD experiment at 1150 K, this pathway is less than 10%.[11]

Excited Electronic State Decomposition. With regard to the discussion of the excited electronic state decomposition of DMNA, a comparison between the computed vertical excitation energies and the experimental excitation energies has been done in order to assess which excited states are relevant to our experimental observations. The vertical excitation energies (E_{vert}) for DMNA, calculated at their CASSCF(10,7)/6-31G(d) optimized FC geometry (ground state minimum) of C_1 symmetry are listed in Table 2. The CASSCF calculations show that the three lowest-lying excited states for DMNA are (n,π^*), (n,π^*), and (π,π^*) states, which correspond to S_1, S_2, and S_3 excited electronic states, respectively. The calculated vertical excitation energies of the S_2(n,π^*), and S_3 (π,π^*) states are 5.65 and 6.6 eV (see Table 2), respectively, which are in good agreement with the experimental values of 5.39 and 6.42 eV.[36] This comparison reveals that dynamical correlation (omitted in a CASSCF calculation but included in MP2 correlated CASSCF calculations) is not the major contributor to these excited electronic states. In addition, the CASSCF computation with a (10,7) active space gives a reasonable treatment of the relevant excited states. By comparison of the excitation energies (5.49 eV at 226 nm, 6.4 eV at 193 nm) used in this work with the calculated vertical excitation energies (5.65 and 6.6 eV, Table 2) of the S_2 (n,π^*) and S_3 (π,π^*) exited states of DMNA, one finds that DMNA is excited to its S_2 (n,π^*) and S_3 (π,π^*) excited states by 226 and 193 nm excitation wavelengths, respectively. Here, we explore only S_0, S_1, and S_2 electronic surfaces of DMNA theoretically in order to explain our experimental results obtained at 226 nm photoexcitation; however, as photodecomposition behavior of DMNA does not change at 193 and 226 nm photoexcitations (see Experimental Results and Discussion), we anticipate similar behavior for S_3 state, which is involved at 193 nm photoexcitation.

A schematic one-dimensional projection of the multidimensional singlet potential energy surfaces (S_0, S_1, and S_2) of DMNA with locations and structures of different critical points is plotted in Figure 10. Path arrows in this figure indicate the classical trajectory of the possible decomposition pathway for the excited electronic state decomposition of DMNA. Potential energy curves are explicitly calculated using IRC algorithm. Computed curves are given in Figures 2−5 of Supporting Information.

The optimized ground state geometry (FC geometry) of DMNA has a nonplanar arrangement of the CNNO moiety (see Figure 10). Above the ground state surface, two stationary points

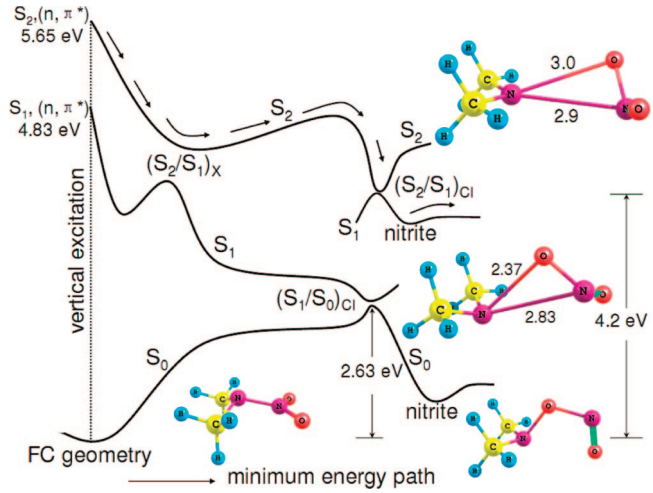

Figure 10. One-dimensional projection of the multidimensional electronic potential energy surfaces of DMNA computed at the CASSCF(10,7)/6-31G(d) level of theory. Note that the $(S_2/S_1)_X$ conical intersection is strongly coupled and that the adiabatic energy gap near this conical intersection is computed to be 485 cm^{-1}. $(S_2/S_1)_{CI}$ and $(S_1/S_0)_{CI}$ are relatively weakly coupled conical intersections. Path arrows represent the classical trajectory of the plausible excited electronic state decomposition mechanism of DMNA.

are localized: (1) a transition state on the S_1 surface and (2) a minimum on the S_2 surface. In addition, three conical intersections between singlet surfaces can be localized: (1) $(S_1/S_0)_{CI}$, conical intersection between S_1 and S_0 surfaces; (2) $(S_2/S_1)_X$, conical intersection between S_2 and S_1 surfaces at short N−N bond distance; (3) $(S_2/S_1)_{CI}$ conical intersection between S_2 and S_1 surfaces at long N−N bond distance. The structure of DMNA at both $(S_1/S_0)_{CI}$ and $(S_2/S_1)_{CI}$ represents a loose geometry in which the NO_2 moiety interacts with the $(CH_3)_2N$ moiety from a long distance (∼2.8 Å). The relative CASSCF energies of the conical intersections on both excited and ground singlet potential energy surfaces of DMNA with respect to the energy of ground state FC geometry are listed in Table 2.

On the basis of the results presented above, we can make different plausible pictures of the dissociation mechanism and dynamics for DMNA. By comparison of vertical excitation energies of different singlet excited electronic states (see Table 2), one can infer that irradiation of isolated molecular DMNA at 226 nm can populate the S_2 state and at 193 nm can populate the S_3 state. As can be seen in Figure 10, vertical excitation to the FC point in the S_2 state can potentially lead to the nonadiabatic nitro−nitrite isomerization through $(S_2/S_1)_{CI}$ conical intersection. This conical intersection is energetically accessible from the FC point of the S_2 surface, because this point is lower in energy than the vertical excitation to the S_2 surface, and negligible energy barrier exists along this decomposition pathway. After crossing the $(S_2/S_1)_{CI}$ conical intersection, DMNA can be directed either to the isomerization product or to the NO_2 elimination product on the S_1 surface. On the S_1 surface the isomerization channel is calculated to be the minimum energy pathway (see Figure S5 of Supporting Information); note that following the $(S_2/S_1)_{CI}$ on the S_1 surface, a 3 kcal/mol energy barrier exists for the NO_2 elimination pathway, but no energy barrier is found for the nitro−nitrite isomerization channel.

Another possible decomposition pathway from the FC point of the S_2 surface would be nonadiabatic deactivation of the molecule to the S_1 surface through the $(S_2/S_1)_X$ conical intersection. After crossing the $(S_2/S_1)_X$ conical intersection, DMNA

additionally can be directed to another surface crossing, the $(S_1/S_0)_{CI}$ conical intersection. This will finally lead the system to the nitro−nitrite isomerization, which is predicted to be the minimum energy pathway on the ground electronic surface. The actual pathway will depend on different factors, such as the rate of IVR and the rate of nonadiabatic transition through the different conical intersections, which can only be assessed by dynamical calculations, e.g., using multiconfiguration time-dependent Hartree (MCTDH).[37] Nonetheless, a few comments can be made on the most plausible mechanism of excited electronic state decomposition of DMNA.

The rate of nonadiabatic transition through a conical intersection depends on the energy gap between the two adiabatic surfaces. A small (weakly avoided crossing) energy gap enhances the probability of nonadiabatic transition from upper electronic state to the lower electronic state near the conical intersection. The computed energy gap between S_2 and S_1 adiabatic surfaces near $(S_2/S_1)_X$ and $(S_2/S_1)_{CI}$ are 487 and 0.73 cm^{-1}, respectively, at the CASSCF(10,7)/6-31G(d) level of theory. Therefore, in a dynamical sense, the nonadiabatic transition through $(S_2/S_1)_{CI}$ will dominate that through $(S_2/S_1)_X$. As a result, nitro−nitrite isomerization though the $(S_2/S_1)_{CI}$ conical intersection on the S_1 surface may be expected to be the major decomposition channel of DMNA from FC point of S_2 surface.

The conclusion of our theoretical study is thus that along the nitro−nitrite isomerization reaction coordinate, the electronic potential energy surfaces ($S_{0,1,2}$) of DMNA are highly coupled, yielding various conical intersections between two electronic adiabatic surfaces. This provides a direct nonadiabatic minimum energy pathway for a nitro−nitrite isomerization when the molecule evolves from the upper electronic surface to the lower electronic surface. Therefore, if the molecule undergoes a nonadiabatic transition through $(S_2/S_1)_{CI}$, nitro−nitrite isomerization will dominate over NO_2 elimination. This explains why our experimental results corroborate nitro−nitrite isomerization as the primary pathway for the excited electronic state decomposition of DMNA. Note, however, that for the isolated molecule conditions of our experiment, the energy in a DMNA molecule following photoexcitation remains constant until fragmentation occurs. The above results deal only with the partitioning of this energy among the different nuclear degrees of freedom of DMNA.

Similar electronic nonadiabatic effects, however, can hinder the adiabatic nitro−nitrite isomerization pathway on the ground state potential energy surface, as discussed above. The NO_2 elimination reaction coordinate, on the other hand, does not suffer from such an electronic nonadiabatic effect. Therefore, adiabatic NO_2 elimination is expected to dominate over adiabatic nitro−nitrite isomerization on the ground state potential energy surface. This explains why at even high temperature NO_2 elimination is a favorable pathway for thermal decomposition of DMNA.

VII. General Conclusions

In this report we have attempted to describe the current state of knowledge for the decomposition of DMNA. Our focus is on the initial unimolecular decomposition reaction of DMNA under isolated conditions. We have critically judged the different experimental and theoretical results, together with our results, in order to rationalize all the experimental and theoretical findings.

Formation of NO and OH radicals has been studied experimentally following decomposition of DMNA at 226 and 193 nm photoexcitations. Both LIF and TOFMS techniques are used for product detection under molecular beam conditions. Contrary to the previous results on DMNA photodecomposition, neither ground state NO_2 nor excited state NO_2 is experimentally observed to be an excited electronic state decomposition product of DMNA. Instead, nitro−nitrite isomerization followed by elimination of NO is found to be the major decomposition channel of DMNA from excited electronic states with a minor contribution from HONO elimination channel. The approximate branching ratio between nitro−nitrite isomerization and HONO elimination channels is experimentally estimated to be 1:0.04.

The NO_2 elimination and nitro−nitrite isomerization channels are also explored through theoretical calculations at the CASSCF level in order to judge which one would be energetically more favorable over the other in the overall decomposition of DMNA. Present computations show the importance of the $(S_2/S_1)_{CI}$ conical intersection in the nitro−nitrite isomerization reaction coordinate as it provides a direct nonadiabatic decomposition pathway in the excited state through isomerization when DMNA evolves from the FC point of the S_2 state, which is experimentally accessed by 226 nm photoexcitation of DMNA. On the ground electronic surface (during thermal decomposition), however, a similar $(S_1/S_0)_{CI}$ conical intersection hinders the isomerization exit channel due to a very small adiabatic energy gap (11 cm^{-1}) between S_1 and S_0 surfaces near this conical intersection (shown in Figure 9). Thereby, where electronic nonadiabatic effects favor a nitro−nitrite isomerization channel for excited electronic state decomposition of DMNA, the same effect hinders this isomerization channel on the ground electronic surface. The NO_2 elimination reaction coordinate is not hindered in the ground state by such an electronic nonadiabatic effect. As a result, NO_2 elimination is favored in the ground state decomposition of DMNA. In addition, the entropy factor can also favor the NO_2 elimination channel in the thermal decomposition of DMNA at high temperature because this decomposition channel possesses positive entropy of reaction.

Therefore, among four possible initial decomposition mechanisms of DMNA, we conclude that the NO_2 elimination is the primary mechanism for thermal decomposition of DMNA. In the excited electronic state decomposition of DMNA, on the other hand, nitro−nitrite isomerization is the primary decomposition mechanism. Our results successfully corroborate and explain the ground state behavior of DMNA decomposition bringing all the experimental and theoretical results on thermal decomposition of DMNA into agreement. Nonetheless, our results are still in contrast with previous photodecomposition results on DMNA, which suggest that NO_2 elimination is the primary channel of decomposition of DMNA in the excited electronic states.

To bring harmony to all the photodecomposition results, the only logical rationalization we can offer is that different experimental conditions perhaps can change the photodecomposition behavior of DMNA. What is anticipated from our present computational study is that during excited electronic state decomposition of DMNA, nitro−nitrite isomerization takes place near a conical intersection through a loose geometry for which the NO_2 moiety interacts with the $(CH_3)_2N$ moiety from a considerably long distance (∼2.8 Å) through a relatively weak interaction (∼3 kcal/mol). Therefore, if enough vibrational energy is provided to the intermolecular modes of these two moieties during this excited state isomerization process, they can promptly diffuse away and can undergo NO_2 elimination.

At room temperature, molecules are thermally hot (∼300 K). Therefore, hot parent molecules can provide enough vibrational

energy to the intermolecular modes of DMNA that the NO_2 and $(CH_3)_2N$ moieties can diffuse away in spite of their initial close proximity during isomerization, resulting in NO_2 elimination as the major decomposition channel. This might be the plausible reason why decomposition of DMNA, at 248 and 266 nm photoexcitations at room temperature under almost collisionless conditions, renders NO_2 elimination.

In the molecular beam, however, molecules are extraordinarily cold (~1 K), and thus the two moieties NO_2 and $(CH_3)_2N$ can remain in close proximity, rendering nitro−nitrite isomerization as the major decomposition channel. The same is possible even at room temperature in a dense gaseous medium, for which cage effects can again keep the two moieties in the close proximity, resulting in nitro−nitrite isomerization as a major decomposition channel. Both have been observed in our experiments.

Therefore, our general conclusion is that the decomposition of DMNA in excited electronic states takes place mostly through a nitro−nitrite isomerization (loose TS) reaction mechanism. The products of this excited electronic state unimolecular decomposition reaction depend on the experimental conditions, however. Nitro−nitrite isomerization in the excited electronic state happens through a loose geometry near a conical intersection between upper and lower electronic states. If the parent molecule is thermally hot and the decomposition takes place under almost collisionless conditions, the NO_2 elimination channel can be the major decomposition pathway from the excited electronic state. Under molecular beam conditions (very cold parent molecules) or in a dense gaseous medium, however, the nitro−nitrite isomerization channel can be the major decomposition pathway from the excited electronic state. In the ground state (thermal decomposition), on the other hand, NO_2 elimination is the major decomposition channel of DMNA.

Acknowledgment. Army Research Office (ARO) is gratefully acknowledged for the financial support of this research.

Supporting Information Available: Supporting Information includes NO_2 fluorescence emission observed following decomposition of nitromethane at 193 nm and S_0, S_1, and S_2 potential energy curves of DMNA explicitly calculated using IRC algorithm and potential energy surface scan at CASSCF level of theory. This material is available free of charge via the Internet at http://pubs.acs.org.

References and Notes

(1) (a) Tokmarkoff, A.; Fayer, M. D.; Dlott, D. D. *J. Chem. Phys.* **1993**, *97*, 1901. (b) Tarver, C. M. *J. Phys. Chem. A* **1997**, *101*, 4845. (c) Fried, L. E.; Ruggerio, A. J. *J. Phys. Chem.* **1994**, *98*, 9786.

(2) Williams, F. *Adv. Chem. Phys.* **1971**, *21*, 289.

(3) Sharma, J.; Beard, B. C.; Chaykovsky, M. *J. Phys. Chem.* **1991**, *95*, 1209.

(4) Gilman, J. *J. Philos. Mag. B* **1995**, *71*, 1057.

(5) Bernstein, E. R. *Overviews of Recent Research on Energetic materials*; Thompson, D., Brill, T., Shaw, R. , Eds.; World Scientific: NJ, 2004.

(6) Greenfield, M.; Guo, Y. Q.; Bernstein, E. R. *Chem. Phys. Lett.* **2006**, *430*, 277.

(7) Adams, G. F.; Shaw, R. W. *Annu. Rev. Phys. Chem.* **1992**, *43*, 311.

(8) Stewart, P. H.; Jeffries, J. B.; Zellweger, J. M.; McMillen, D. F.; Golden, D. V. *J. Phys. Chem.* **1989**, *93*, 3557. (b) Nigenda, S. E.; McMillen, D. F.; Golden, D. M. *J. Phys. Chem.* **1989**, *93*, 1124.

(9) Lloyd, S. A.; Umstead, M. E.; Lin, M. C. *J. Energ. Mater.* **1985**, *3*, 187.

(10) Flournoy, J. M. *J. Chem. Phys.* **1962**, *36*, 1106.

(11) (a) Lazarou, Y. G.; Papagiannakopoulos, P. *J. Phys. Chem.* **1990**, *94*, 7114. (b) Lazarou, Y. G.; Papagiannakopoulos, P. *Laser Chem.* **1993**, *13*, 101.

(12) McQuaid, M. J.; Miziolek, A. W.; Sausa, R. C.; Merrow, C. N. *J. Phys. Chem.* **1991**, *95*, 2713.

(13) Mialocq, J. C.; Stephenson, J. C. *Chem. Phys. Lett.* **1986**, *123*, 390. (b) Mialocq, J. C.; Stephenson, J. C. *Chem. Phys.* **1986**, *106*, 281.

(14) (a) Lemire, G. W.; Simeonsson, J. B.; Sausa, R. C. *Anal. Chem.* **1993**, *65*, 529. (b) Simeonsson, J. B.; Lemire, G. W.; Sausa, R. C. *Appl. Spectrosc.* **1993**, *11*, 1907.

(15) Guo, Y. Q.; Greenfield, M.; Bhattacharya, A.; Bernstein, E. R. *J. Chem. Phys.* **2007**, *127*, 154301.

(16) (a) Velardez, G. F.; Alavi, S.; Thompson, D. L. *J. Chem. Phys.* **2005**, *123*, 074313. (b) Sumpter, B. G.; Thompson, D. L. *J. Chem. Phys.* **1987**, *86*, 3301. (c) Sumpter, B. G.; Thompson, D. L. *J. Chem. Phys.* **1988**, *88*, 6889.

(17) Saxon, R. P.; Yoshimine, M. *J. Phys. Chem.* **1989**, *93*, 3130.

(18) Seminario, J. M.; Politzer, P. *Int. J. Quantum Chem.* **1992**, *26*, 497.

(19) Mebel, A. M.; Hsu, C. C.; Lin, M. C.; Morokuma, K. *J. Chem. Phys.* **1995**, *103*, 5640.

(20) (a) Soto, J.; Arenas, J. F.; Otero, J. C.; Pelaez, D. *J. Phys. Chem. A* **2006**, *110*, 8221. (b) Arenas, J. F.; Otero, J. C.; Pelaez, D.; Soto, J. *J. Phys. Chem. A* **2005**, *109*, 7172.

(21) Wei, W. M.; Zheng, R. H.; Tian, Y.; He, T. J.; He, L.; Chen, D. M.; Liu, F. C. *Chin. J. Chem. Phys.* **2007**, *27*, 126.

(22) Im, H. S.; Bernstein, E. R. *J. Chem. Phys.* **2000**, *113*, 7911. (b) Guo, Y. Q.; Greenfield, M.; Bernstein, E. R. *J. Chem. Phys.* **2005**, *122*, 244310.

(23) Dong, F.; Heinbuch, S.; Xie, Y.; Rocca, J. J.; Bernstein, E. R.; Wang, Z. C.; Derg, K.; He, S. G. *J. Am. Chem. Soc.* **2008**, *130*, 1932.

(24) Frisch, M. J.; Trucks, G. W.; Schlegel, H. B.; Scuseria, G. E.; Robb, M. A.; Cheeseman, J. R.; Montgomery, J.; Vreven, J. A. T.; Kudin, K. N.; Burant, J. C.; Millam, J. M.; Iyengar, S. S.; Tomasi, J.; Barone, V.; Mennucci, B.; Cossi, M.; Scalmani, G.; Rega, N.; Petersson, G. A.; Nakatsuji, H.; Hada, M.; Ehara, M.; Toyota, K.; Fukuda, R.; Hasegawa, J.; Ishida, M.; Nakajima, T.; Honda, Y. ; Kitao, O.; Nakai, H.; Klene, M.; Li, X.; Knox, J. E.; Hratchian, H. P.; Cross, J. B.; Adamo, C.; Jaramillo, J.; Gomperts, R.; Stratmann, R. E.; Yazyev, O.; Austin, A. J.; Cammi, R.; Pomelli, C.; Ochterski, J. W.; Ayala, P. Y.; Morokuma, K.; Voth, G. A.; Salvador, P.; Dannenberg, J. J.; Zakrzewski, V. G.; Dapprich, S.; Daniels, A. D.; Strain, M. C.; Farkas, O.; Malick, D. K.; Rabuck, A. D.; Raghavachari, K.; Foresman, J. B.; Ortiz, J. V.; Cui, Q.; Baboul, A. G.; Clifford, S.; Cioslowski, J.; Stefanov, B. B.; Liu, G.; Liashenko, A.; Piskorz, P.; Komaromi, I.; Martin, R. L.; Fox, D. J.; Keith, T.; Al-Laham, M. A.; Peng, C. Y.; Nanayakkara, A.; Challacombe, M.; Gill, P. M. W.; Johnson, B.; Chen, W.; Wong, M. W.; Gonzalez, C.; Pople, J. A. *GAUSSIAN 03*, revision B.04; Gaussian, Inc., Pittsburgh, PA, 2003.

(25) Simeonsson, J. B.; Sausa, R. C. *Appl. Spec. Rev.* **1996**, *31*, 1.

(26) Guo, Y. Q.; Bhattacharya, A.; Bernstein, E. R. *J. Phys. Chem. A* **2008**, accepted.

(27) (a) Hippler, M.; Pfab, J. *Chem. Phys. Lett.* **1995**, *243*, 500. (b) Herzberg, G. *Spectra of Diatomic Molecules*; Van Nostrand: New York, 1950; p 257.

(28) (a) Im, H. S.; Bernstein, E. R. *J. Phys. Chem. A* **2002**, *106*, 7565. (b) Wikinson, I.; Whitaker, B. J. *J. Chem. Phys.* **2008**, *129*, 154312.

(29) Donnelly, V. M.; Kaufman, F. *J. Chem. Phys.* **1978**, *69*, 1456.

(30) McKendrick, C. B.; Fotakis, C.; Donovan, R. J. *J. Photochem.* **1982**, *20*, 175.

(31) Butler, L. J.; Krajnovich, D.; Lee, Y. T.; Ondrey, G.; Bersohn, R. *J. Chem. Phys.* **1983**, *79*, 1708.

(32) See ref 27b, p 125.

(33) Levine, R. D. *Molecular Reaction Dynamics*; Cambridge University Press: Cambridge, UK, 2005; p 264.

(34) Zener, C. *Proc. R. Soc London, Ser. A* **1932**, *137*, 696.

(35) (a) Person, M. D.; Kash, P. W.; Butler, L. J. *J. Chem. Phys.* **1992**, *97*, 355. (b) Butler, L. J.; Neumark, D. M. *J. Phys. Chem.* **1996**, *100*, 801.

(36) McQuaid, M. J.; Sausa, R. C. *Appl. Spectrosc.* **1991**, *45*, 916.

(37) Worth, G. A.; Cederbaum, L. S. *Annu. Rev. Phys. Chem.* **2004**, *55*, 127.

JP807247T